Magnetism in semiconductors: A dynamical mean-field study of ferromagnetism in $Ga_{1-x}Mn_xAs$

K. Aryanpour,[1,3] J. Moreno,[2,3] M. Jarrell,[3] and R. S. Fishman[4]
[1]*Department of Physics, University of California, Davis, California 95616, USA*
[2]*Department of Physics and Astronomy, Clemson University, Clemson, South Carolina 29634, USA*
[3]*Department of Physics, University of Cincinnati, Cincinnati, Ohio 45221, USA*
[4]*Condensed Matter Sciences Division, Oak Ridge National Laboratory, Oak Ridge, Tennessee 37831, USA*
(Received 9 November 2004; revised manuscript received 29 March 2005; published 19 July 2005)

We employ the dynamical mean-field approximation to perform a systematic study of magnetism in $Ga_{1-x}Mn_xAs$. Our model incorporates the effects of the strong spin-orbit coupling on the $J=\frac{3}{2}$ GaAs valence bands and of the exchange interaction between the randomly distributed magnetic ions and the itinerant holes. The ferromagnetic phase transition temperature T_c is obtained for different values of the impurity-hole coupling J_c and of the hole concentration n_h at the Mn doping of $x=0.05$. We also investigate the temperature dependence of the local magnetization and spin polarization of the holes. By comparing our results with those for a single band Hamiltonian, we conclude that the spin-orbit coupling in $Ga_{1-x}Mn_xAs$ gives rise to frustration in the ferromagnetic order, strengthening recent findings by Zaránd and Jankó [Phys. Rev. Lett. **89**, 047201 (2002)].

DOI: 10.1103/PhysRevB.72.045343 PACS number(s): 75.50.Pp, 02.70.−c, 05.10.−a, 71.27.+a

I. INTRODUCTION

The discovery of ferromagnetism in GaAs doped with Mn has renewed interest in the properties of diluted magnetic semiconductors.[1] Since these materials are good sources of polarized holes, they may form the basis of *spintronics* devices[2] that employ both the spin and the charge of the carrier to convey information.

In $Ga_{1-x}Mn_xAs$, the Mn ions are in the Mn^{2+} state with a half-filled d shell of total spin $S=\frac{5}{2}$.[3,4] Since Mn^{2+} ions primarily replace Ga^{3+}, they act as effective acceptors by supplying holes as well as localized spins. The valence band of pure GaAs is p-like so the strong spin-orbit interaction couples the $l=1$ angular momentum of the p orbitals to the electron spin $\left(s=\frac{1}{2}\right)$, resulting in a total spin $J=l+s=\frac{3}{2}$ for the valence holes.[5] As discussed by Zaránd and Jankó,[6] the strong spin-orbit coupling also induces an *anisotropic* carrier-mediated interaction between the Mn ions and, as a consequence, frustration in their ferromagnetic order. While the results of Ref. 6 were limited to the metallic regime and to small values of the Mn-hole coupling, a different approach suggests the presence of an impurity band in the dilute limit.[7]

In this article, we employ the dynamical mean-field approximation (DMFA)[8–11] to perform a systematic analysis of ferromagnetism in $Ga_{1-x}Mn_xAs$, including the effects of strong spin-orbit coupling on the $J=\frac{3}{2}$ GaAs valence band. The DMFA includes the spin-split impurity band through quantum self-energy corrections, which are not included in other mean-field theories. Because this method is nonperturbative, it allows us to study both the metallic and impurity-band regimes as well as both small and large couplings. We show how the spin-orbit interaction affects the ferromagnetic critical temperature T_c, the hole polarization, and the Mn magnetization. By comparing our results with those for a single band Hamiltonian without spin-orbit coupling, we conclude that strong spin-orbit coupling in $Ga_{1-x}Mn_xAs$ produces frustration for all coupling strengths. For carrier concentrations smaller than the doping, both T_c and the polarization of the carriers are reduced for all values of the coupling. For larger carrier densities and large couplings, we unexpectedly find that frustration induces a small but finite T_c, in sharp contrast with the vanishing T_c found when the spin-orbit is neglected.

II. MODEL

Our starting point is the simplified Hamiltonian proposed in Ref. 6: $H=H_0-J_c\Sigma_{R_i}\mathbf{S}_i\cdot\hat{\mathbf{J}}(R_i)$. The first term includes the electronic dispersion and the spin-orbit coupling of the $J=\frac{3}{2}$ valence holes within the spherical approximation.[12] The second term is the dominant part of the interaction between the Mn spins and the valence holes,[13] with J_c the exchange coupling and $\hat{\mathbf{J}}(R_i)$ the total $J=\frac{3}{2}$ spin density of the holes at the site i of a Mn ion with spin $\mathbf{S}_i$. The relatively large magnitude of the Mn local moment justifies a classical treatment of its spin.

Within the spherical approximation,[12] the Hamiltonian of pure GaAs is rotationally invariant. Hence, H_0 is diagonal in a *chiral* basis, $H_0=\Sigma_{\mathbf{k},\gamma}(k^2/2m_\gamma)\tilde{c}^\dagger_{\mathbf{k}\gamma}\tilde{c}_{\mathbf{k}\gamma}$, where $\tilde{c}^\dagger_{\mathbf{k},\gamma}$ creates a chiral hole with momentum $\mathbf{k}$ parallel to its spin and $\hat{\mathbf{J}}\cdot\hat{\mathbf{k}}=\pm\frac{3}{2}$ or $\pm\frac{1}{2}$. The two band masses $m_h\approx 0.5m$ and $m_l\approx 0.07m$ correspond to the heavy and light bands with $\gamma=\pm\frac{3}{2}$ and $\pm\frac{1}{2}$, respectively (m is the electron mass).

Unfortunately, the exchange interaction term obtains a rather complicated momentum-dependent form in the chiral basis[6] that is responsible for the frustrated order of the Mn. The competition between the strong spin-orbit coupling on the hole bands, which aligns the hole spin parallel to its momentum, and the exchange interaction with the local moment, which aligns the hole and local spins, prevents all of the carrier density from mediating the magnetic order.

We develop a DMFA algorithm that takes advantage of the simple diagonal form of H_0 in the chiral basis and the

local form of the exchange interaction in the nonchiral basis. The coarse-grained Green function matrix in the nonchiral fermion basis is

$$\hat{\bar{G}}(i\omega_n) = \frac{1}{N}\sum_{\mathbf{k}} [i\omega_n \hat{I} - \hat{\epsilon}(k) + \mu\hat{I} - \hat{\bar{\Sigma}}(i\omega_n)]^{-1}, \qquad (1)$$

where N is the number of $\mathbf{k}$ points in the first Brillouin zone and $\hat{\epsilon}(k)=\hat{R}^{\dagger}(\hat{\mathbf{k}})(k^2/2m_{\gamma})\hat{R}(\hat{\mathbf{k}})$ is the dispersion in the spherical approximation. Here, $\hat{R}$ are spin $\frac{3}{2}$ rotation matrices that relate the fermion operator, $c_{\mathbf{k}\gamma}$, to its chiral counterpart, $\tilde{c}_{\mathbf{k}\gamma}=R_{\gamma\nu}(\hat{\mathbf{k}})c_{\mathbf{k}\nu}$. The mean-field function $\hat{\mathcal{G}}_0(i\omega_n)=[\hat{\bar{G}}^{-1}(i\omega_n)+\hat{\bar{\Sigma}}(i\omega_n)]^{-1}$ is required to solve the DMFA impurity problem. At a nonmagnetic site, the local Green function equals the mean-field function, $\hat{G}_{non}=\hat{\mathcal{G}}_0$. By treating disorder in a fashion similar to the *coherent potential approximation* (CPA)[14] for a given local spin configuration, we obtain the local Green function at a magnetic site: $\hat{G}_{mg}(i\omega_n)=[\hat{\mathcal{G}}_0^{-1}(i\omega_n)+J_c\mathbf{S}\cdot\hat{\mathbf{J}}]^{-1}$.

Now $\hat{G}_{mg}(i\omega_n)$ must be averaged over all possible spin orientations at the local site and over all possible impurity configurations on the lattice. The former is implemented by using the effective action[15]

$$S_{eff}(\mathbf{S}) = -\sum_n \log\det[\mathcal{G}_0(i\omega_n)(\mathcal{G}_0^{-1}(i\omega_n) + J_c\mathbf{S}\cdot\hat{\mathbf{J}})]e^{i\omega_n 0^+} \qquad (2)$$

to average over the angular distribution of the local spins:

$$\langle\hat{G}_{mg}(i\omega_n)\rangle = \frac{1}{\mathcal{Z}}\int d\Omega_{\mathbf{S}}\hat{G}_{mg}(i\omega_n)\exp[-S_{eff}(\mathbf{S})], \qquad (3)$$

where $\mathcal{Z}=\int d\Omega_{\mathbf{S}}\exp[-S_{eff}(\mathbf{S})]$. The extra factor of $\hat{\mathcal{G}}_0(i\omega_n)$ in Eq. (2) does not change the physics, but it is introduced to aid in convergence. If the Mn ions are randomly distributed with probability x, the configurationally averaged Green function reads $\hat{G}_{avg}(i\omega_n)=\langle\hat{G}_{mg}(i\omega_n)\rangle x+\hat{\mathcal{G}}_0(i\omega_n)(1-x)$. A more elaborate discussion on solving the impurity problem is given in Appendix A.

Finally, the magnetization of the Mn ions can be calculated as

$$M^z = \frac{1}{\mathcal{Z}}\int d\Omega_{\mathbf{S}}S^z\exp\{-[S_{eff}(\mathbf{S}) - \beta\mathbf{S}\cdot\delta\mathbf{H}^z]\}, \qquad (4)$$

where a small magnetic field $\delta\mathbf{H}^z$ is applied to break the symmetry along a preferential direction, i.e., the z axis. By fitting the magnetization $M^z(T)$ in the vicinity of the transition to a static mean-field form, we can extract the value of T_c for each set of parameters studied. Appendix B contains a detailed discussion of how T_c is extracted from the magnetization data.

III. RESULTS

We focus on the doping of $x=0.05$ for which T_c is between the highest reported.[16–22] The spin-orbit coupling is responsible for the splitting between the $J=\frac{3}{2}$ and the $J=\frac{1}{2}$ bands and for the chiral nature of the $J=\frac{3}{2}$ holes. However, the chirality can be turned off by making the heavy and light hole masses equal, while still preserving the split-off gap. In order to clearly elucidate the role played by the spin-orbit coupling, we introduce two parameters. One is the hole mass of an equivalent system composed of two degenerate bands with the same average kinetic energy as our system: $2m_{eq}^{3/2}=m_h^{3/2}+m_l^{3/2}$. The other is the ratio of light and heavy hole effective masses, $\alpha=m_l/m_h$. The chirality can be switched off by setting $\alpha=1$ while keeping m_{eq} constant.

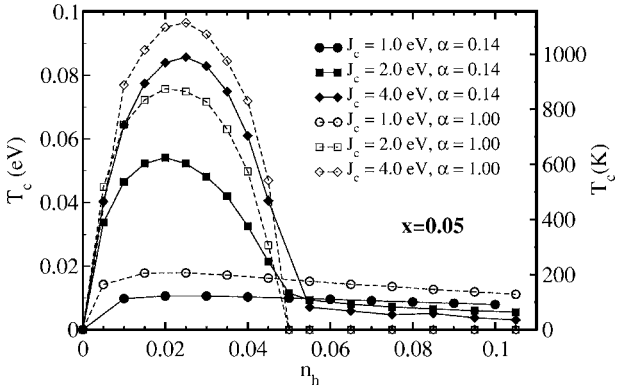

FIG. 1. The phase transition temperature T_c versus carrier concentration n_h for Mn doping $x=0.05$, various J_c values, and effective mass ratios, α.

Figure 1 presents our results for the phase transition temperature T_c as a function of the hole concentration n_h for a fixed Mn concentration, $x=0.05$, and for various values of J_c and α. There are two regimes corresponding to small and large values of the interaction strength, J_c. For large J_c, the holes form bound states with the Mn impurities, an impurity band develops inside the GaAs gap, and the properties of the host are greatly affected. The value of J_c at which the impurity band appears depends upon the value of α.

First consider the nonchiral case with $\alpha=1.0$ so that the spin-orbit coupling is turned off within the $J=\frac{3}{2}$ bands. For $J_c=1.0$ eV the system is far from the impurity-band regime and T_c has a relatively slow variation with respect to n_h. For $J_c=2.0$ eV the system is beyond the threshold for the formation of an impurity band, which then dominates the physics. The maximum T_c occurs when the impurity band is nearly half filled ($n_h\approx x/2$).[23] For $J_c=4.0$ eV the impurity band is well established and the maximum T_c is large. Because ferromagnetic order restricts the hopping of holes when the impurity band is full, T_c vanishes for $J_c>1.0$ eV and $n_h>x$.

An antiferromagnetic ground state is energetically more favorable in the regime $n_h>x$ (Ref. 23) because the carriers can then easily hop from one impurity site to another. Magnetization curves in Fig. 2 for $J_c=2.0$ and 4.0 eV and $n_h>x$ provide evidence for antiferromagnetism. They fit a Curie-Weiss functional form, $M^z=M_0^z/(1+T/T_\theta)$ with a positive T_θ ranging from 40 to 117 K, indicating antiferromagnetic order for $\alpha=1.0$ and $n_h>x$.

We now consider the chiral case with $\alpha=0.14$, the ratio between light and heavy hole masses in GaAs. The effects of frustration on the ferromagnetic critical temperature are

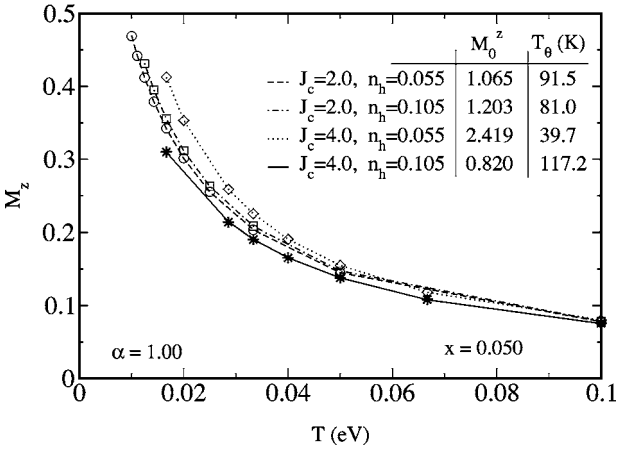

FIG. 2. The magnetization versus temperature for $\alpha=1.0$ and $n_h>\mathbf{x}=0.05$ at $J_c=2.0$ eV and $n_h=0.055$ (dashed line and circles), $J_c=2.0$ eV and $n_h=0.105$ (dot-dashed line and squares), $J_c=4.0$ eV and $n_h=0.055$ (dotted line and diamonds), and $J_c=4.0$ eV and $n_h=0.105$ (solid line and stars). The curves are the Curie law fits with positive T_θ values.

readily seen in Fig. 1. For $J_c=1.0$ eV, T_c consistently lies below its nonchiral counterpart. At $J_c=2.0$ and 4.0 eV, the difference between the chiral and nonchiral results is even larger. For $n_h<x$, the nonchiral T_c is always higher than the chiral T_c. However, for $n_h>x$, the chiral results continue to yield a finite although greatly diminished T_c in the same regime where T_c vanished when $\alpha=1.0$. Surprisingly, the ferromagnetic T_c survives at large doping due to the intrinsic frustration in the system. Strong spin-orbit scattering allows the impurity-band carriers to hop between impurity sites that are ferromagnetically aligned even when the impurity band is full, thereby stabilizing the magnetic order. This novel result indicates that frustration always acts to destabilize the magnetically ordered phase favored in the absence of frustration.

The formation of an impurity band is responsible for many of the outstanding properties of this system. Impurity-band formation appears as a discontinuity of the hole chemical potential μ at $n_h=x$. Figure 3 depicts μ vs. n_h for $T=0.05$ eV (580 K) and for the same values of J_c and α used in Fig. 1. The presence of an impurity band depends on both

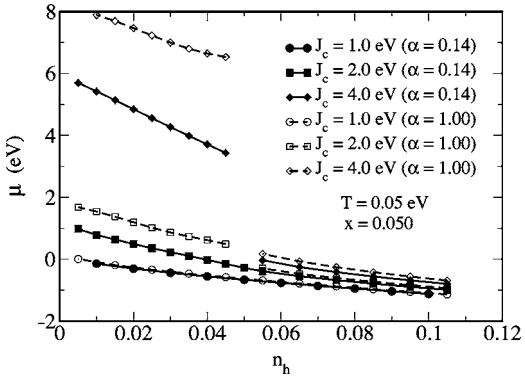

FIG. 3. The chemical potential, μ, versus n_h for Mn doping $x=0.05$ and $T=0.05$ eV using the same values of J_c and α as in Fig. 1.

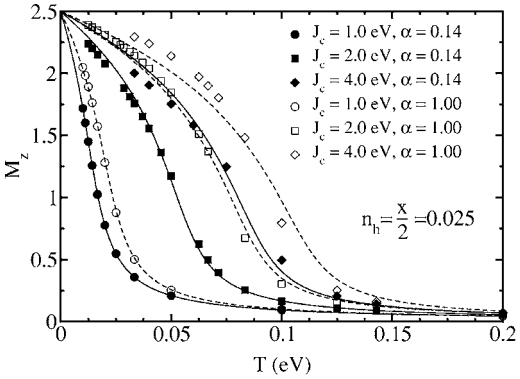

FIG. 4. The magnetization versus temperature for different chirality modes and different values of J_c at $n_h=x/2=0.025$ and $\delta H^z=0.004$ eV. The curves are the static mean field fits with T_c values equal to those given by our results: solid curves fit the results for $\alpha=0.14$, dashed curves the ones for $\alpha=1$.

J_c and α. When $J_c=1.0$, no impurity band is present so the chiral and nonchiral μ are almost identical and neither shows a discontinuity. When $J_c=2.0$ eV and $\alpha=1.0$, the impurity band has already split from the valence band. At the same value of $J_c=2.0$ eV but when $\alpha=0.14$, the change in slope of μ at $n_h=x$ indicates that the impurity band is present but that it overlaps with the main band. When $J_c=4.0$ eV and $\alpha=0.14$, the hole chemical potential is discontinuous at $n_h=x$, signaling the splitting of the impurity band from the valence band. For these larger values of J_c, the nonchiral μ always lies below the chiral value, indicating that the nonchiral impurity band lies at lower energies than the chiral one. Since the interaction between the impurity moments is mediated by the host of holes, the less pronounced impurity band for $\alpha=0.14$ is another signature of the frustration produced by chirality. Notice that for large values of J_c the impurity band drifts to energy values larger than the semiconducting gap. In this case the conduction band might become as relevant as the split-off band in the modeling of magnetic semiconductors.

Optical conductivity measurements[24] show that the impurity band is split from the valence band at the doping of $x=0.05$. This fact and our results for T_c suggest a value of J_c comparable to the values obtained with photoemission techniques[4] and infrared spectroscopy.[3,25]

The magnetization also reveals the effects of frustration. In Fig. 4, the temperature dependence of the magnetization is plotted for $n_h=x/2=0.025$. Our results are compared with Curie-Weiss fits for the same T_c values. When $J_c=1.0$ eV, the mean-field curves perfectly fit the data not only at large temperatures but also below T_c. But for larger J_c values and low temperatures, discrepancies appear between the static mean-field curves and the DMFA results. For $\alpha=1.0$, the magnetization in our model lies above the mean-field Heisenberg magnetization when $T<T_c$ since the scattering between the itinerant carriers and the localized spins becomes coherent at low temperatures, thereby enhancing the magnetic order of the local ions. This effect has also been seen in the double exchange model.[26] However, for $\alpha=0.14$, frustration reduces the low-temperature coherence between the carriers and local ions. So when $T<T_c$, the magnetiza-

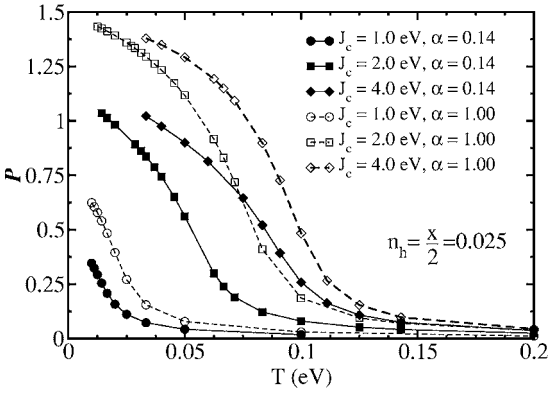

FIG. 5. The hole polarization $\mathcal{P}$ versus temperature at $n_h=x/2=0.025$ and $\delta H^z=0.004$ eV.

tion curves lie below the mean-field Heisenberg predictions.

Lastly, we study the carrier spin polarization, $\mathcal{P}$, which is constructed from appropriate sums of the Green function. Control of $\mathcal{P}$ is important for *spintronics* applications, since the spin polarization of the holes is required to transport information. Figure 5 illustrates the temperature dependence of the hole polarization when $n_h=x/2=0.025$ for several values of J_c and α. For all J_c values, chirality suppresses the polarization. For $\alpha=1.0$, large J_c, and low temperatures, $\mathcal{P}$ approaches $\frac{3}{2}$ since all holes occupy the lowest energy level with $j_z=+\frac{3}{2}$. But due to frustration even for large J_c and low temperatures, $\mathcal{P}$ for $\alpha=0.14$ is significantly smaller. This agrees with previous calculations of the zero-temperature polarization, where the destructive effects of the spin-orbit interaction were also found.[27]

IV. CONCLUSIONS

In summary, we have studied the diluted magnetic semiconductor $Ga_{1-x}Mn_xAs$ using a nonperturbative multi-orbital DMFA algorithm incorporating the effects of the strong spin-orbit coupling. We have calculated the ferromagnetic critical temperature, hole chemical potential, local ion magnetization, and hole polarization for a broad range of model parameters. We find that the spin-orbit coupling leads to frustration and reduced magnetization when the hole concentration n_h is smaller than the impurity concentration x, in agreement with previous perturbative calculations.[6] In addition, we find that this behavior persists for large values of J_c, and that frustration greatly reduces the transition temperature T_c and the polarization of the carriers for all J_c. Finally, when J_c is large, we find the surprising result that frustration induces a region of finite T_c for $n_h>x$.

This approach has promising future developments. It can be extended to study other magnetic semiconductors and realistic devices such as semiconducting heterostructures and quantum dot systems, which can be tailored to take full advantage of the intrinsic anisotropy of the ferromagnetic order. More sophisticated approaches, such as the dynamical cluster approximation (DCA),[28] may be used to go beyond the single-site approximation and explore the cooperative and glassy effects of frustration, such as the reduction in the local magnetization at low temperatures.

ACKNOWLEDGMENTS

We acknowledge useful conversations with N. Furukawa and B. Jankó. This research was supported by NSF Grant Nos. DMR-0073308 and DMR-0312680 and by the Department of Energy Grant Nos. DE-FG02-01ER45897 and DE-FG03-03NA00071 (SSAAP program) and also under Contract No. DE-AC05-00OR22725 with Oak Ridge National Laboratory, managed by UT-Battelle, LLC.

APPENDIX A: THE DMFA SELF-CONSISTENT TREATMENT OF THE IMPURITY PROBLEM

In this problem, the interacting part of the Hamiltonian in the nonchiral basis, namely, $H_{int}=\Sigma_{R_i}\hat{V}_i=-J_c\Sigma_{R_i}\mathbf{S}_i\cdot\hat{\mathbf{J}}(R_i)$, is a local interaction. However, in the chiral basis the interaction becomes nonlocal, $\hat{V}_i^{ch}=\hat{V}_i^{ch}(\mathbf{k},\mathbf{k}')=\hat{R}(\hat{\mathbf{k}})\hat{V}_i\hat{R}^{\dagger}(\hat{\mathbf{k}}')$.

We treat the self-energy diagrammatics for the impurity problem in the chiral basis in a fashion similar to the *coherent potential approximation* (CPA),[14] as illustrated in Fig. 6.

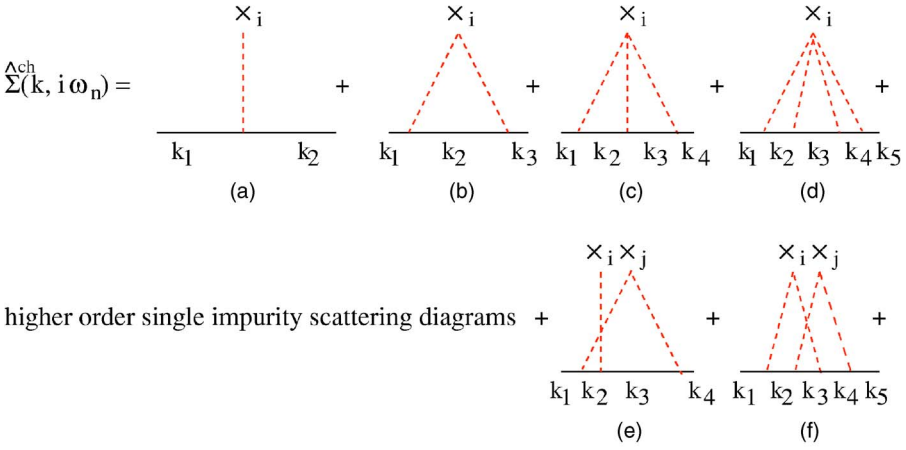

FIG. 6. (Color online) The irreducible Feynman diagrammatics for the self-energy in the chiral basis. x_i and x_j are single Mn impurities residing at sites i and j, respectively. Solid lines are one-particle cluster excluded hole Green function matrices $\hat{\mathcal{G}}_0^{ch}(\mathbf{k},i\omega_n)$ in the chiral basis and dashed lines are impurity-hole interaction matrices $\hat{V}^{ch}(\mathbf{k},\mathbf{k}')$. Diagrams (a)–(d) all correspond to single impurity scattering. Diagrams (e) and (f) are irreducible self-energy diagrams associated with scattering off two different impurity sites and vanish in the DMFA.

We need to average over all the possible configurations of Mn impurity atoms to restore the lattice translational invariance. As a result, each impurity site denoted by x_i or x_j gets renormalized by an impurity concentration factor x. For the moment, we assume that there is an impurity atom on every site of the lattice and therefore $x=1$. Solid lines are one-particle cluster excluded hole Green function matrices $\mathcal{G}_0^{ch}(\mathbf{k},i\omega_n)$ in the chiral basis and dashed lines are impurity-hole interaction matrices $\hat{V}^{ch}(\mathbf{k},\mathbf{k}')$ (the index i drops as we average over the entire impurity configurations on the lattice). We also sum over all internal momenta while conserving the total momentum at every internal vertex. Thus, for instance, the self-energy contribution corresponding to diagram (c) in Fig. 6 reads

$$\hat{\Sigma}_{(c)}^{ch}(\mathbf{k}_1,i\omega_n)=\frac{1}{N^2}\delta_{\mathbf{k}_1,\mathbf{k}_4}\sum_{\mathbf{k}_2,\mathbf{k}_3}\hat{V}^{ch}(\mathbf{k}_1,\mathbf{k}_2)\mathcal{G}_0^{ch}(\mathbf{k}_2,i\omega_n)\times\hat{V}^{ch}(\mathbf{k}_2,\mathbf{k}_3)\mathcal{G}_0^{ch}(\mathbf{k}_3,i\omega_n)\hat{V}^{ch}(\mathbf{k}_3,\mathbf{k}_4). \tag{A1}$$

For two-impurity crossing diagrams such as diagram (f) in Fig. 6, one must subtract the contribution due to sites $i=j$ to avoid over counting as shown below:

$$\hat{\Sigma}_{(f)}^{ch}(\mathbf{k}_1,i\omega_n)=\frac{1}{N^3}\delta_{\mathbf{k}_1,\mathbf{k}_5}\left[\sum_{\mathbf{k}_2,\mathbf{k}_3,\mathbf{k}_4}\hat{V}^{ch}(\mathbf{k}_1,\mathbf{k}_2)\mathcal{G}_0^{ch}(\mathbf{k}_2,i\omega_n)\hat{V}^{ch}(\mathbf{k}_2,\mathbf{k}_3)\mathcal{G}_0^{ch}(\mathbf{k}_3,i\omega_n)\hat{V}^{ch}(\mathbf{k}_3,\mathbf{k}_4)\mathcal{G}_0^{ch}(\mathbf{k}_4,i\omega_n)\hat{V}^{ch}(\mathbf{k}_4,\mathbf{k}_5)\delta_{\mathbf{k}_2-\mathbf{k}_3,\mathbf{k}_5-\mathbf{k}_4}-\frac{1}{N}\left(\sum_{\mathbf{k}_2,\mathbf{k}_3,\mathbf{k}_4}\hat{V}^{ch}(\mathbf{k}_1,\mathbf{k}_2)\mathcal{G}_0^{ch}(\mathbf{k}_2,i\omega_n)\hat{V}^{ch}(\mathbf{k}_2,\mathbf{k}_3)\mathcal{G}_0^{ch}(\mathbf{k}_3,i\omega_n)\hat{V}^{ch}(\mathbf{k}_3,\mathbf{k}_4)\mathcal{G}_0^{ch}(\mathbf{k}_4,i\omega_n)\hat{V}^{ch}(\mathbf{k}_4,\mathbf{k}_5)\right)\right]. \tag{A2}$$

In the DMFA, we freely sum over all internal momenta in the Feynman diagrams relinquishing the total momentum conservation at internal vertices.[9] In order to implement this in diagram (f) of Fig. 6, it is sufficient to set $\delta_{\mathbf{k}_2-\mathbf{k}_3,\mathbf{k}_5-\mathbf{k}_4}\rightarrow 1/N$, which leads to

$$\hat{\Sigma}^{(f)}(\mathbf{k}_1,i\omega_n)=0 \quad \left(\delta_{\mathbf{k}_2-\mathbf{k}_3,\mathbf{k}_5-\mathbf{k}_4}\rightarrow\frac{1}{N}\right). \tag{A3}$$

Since the above result can be generalized to all multiple impurity diagrams, we find that only the single impurity diagrams survive. In addition, as proven ahead, all the Green functions and interactions in the self-energy diagrams can now be mapped back to the nonchiral basis where they are local.

Knowing that the interactions in the nonchiral basis are local, we find

$$\mathcal{G}_0^{ch}(\mathbf{k},i\omega_n)=\hat{R}(\hat{\mathbf{k}})\mathcal{G}_0(\mathbf{k},i\omega_n)\hat{R}^{\dagger}(\hat{\mathbf{k}}). \tag{A4}$$

Hence, Eq. (A1) can be rewritten as

$$\hat{\Sigma}_{(c)}^{ch}(\mathbf{k}_1,i\omega_n)=\frac{1}{N^2}\delta_{\mathbf{k}_1,\mathbf{k}_4}\sum_{\mathbf{k}_2,\mathbf{k}_3}\hat{R}(\hat{\mathbf{k}}_1)\hat{V}\hat{R}^{\dagger}(\hat{\mathbf{k}}_2)\times\hat{R}(\hat{\mathbf{k}}_2)\mathcal{G}_0(\mathbf{k}_2,i\omega_n)\hat{R}^{\dagger}(\hat{\mathbf{k}}_2)\hat{R}(\hat{\mathbf{k}}_2)\hat{V}\hat{R}^{\dagger}(\hat{\mathbf{k}}_3)\hat{R}(\hat{\mathbf{k}}_3)\times\mathcal{G}_0(\mathbf{k}_3,i\omega_n)\hat{R}^{\dagger}(\hat{\mathbf{k}}_3)\hat{R}(\hat{\mathbf{k}}_3)\hat{V}\hat{R}^{\dagger}(\hat{\mathbf{k}}_4). \tag{A5}$$

Since $\hat{R}^{\dagger}(\hat{\mathbf{k}})\hat{R}(\hat{\mathbf{k}})=1$

$$\hat{\Sigma}_{(c)}^{ch}(\mathbf{k}_1,i\omega_n)=\delta_{\mathbf{k}_1,\mathbf{k}_4}\hat{R}(\hat{\mathbf{k}}_1)\hat{\Sigma}(i\omega_n)\hat{R}^{\dagger}(\hat{\mathbf{k}}_4). \tag{A6}$$

So, to all orders the DMFA self-energy in the chiral basis can be simply mapped onto the local nonchiral self-energy by a backward rotation from $\hat{\mathbf{k}}$ axis to z axis. The simplification achieved by the DMFA allows us to sum all single impurity Green function diagrams to infinite orders. The local impurity Green function is defined in a CPA manner:

$$\hat{G}_{imp}(i\omega_n)=[\hat{\mathcal{G}}_0^{-1}(i\omega_n)+J_c\mathbf{S}\cdot\hat{\mathbf{J}}]^{-1}. \tag{A7}$$

$\hat{G}_{imp}(i\omega_n)$ needs to be averaged over all possible impurity spin orientations at a single impurity site. This task is implemented by Eq. (3).

Earlier while discussing the impurity scattering self-energy, we assumed that $x=1$. If $x<1$, we need to average over all possible impurity configurations as well. For sites with no impurity atoms, $\hat{G}_{imp}(i\omega_n)=\hat{\mathcal{G}}_0(i\omega_n)$. Thus, the total configurationally averaged Green function reads

$$\hat{G}_{avg}(i\omega_n)=\langle\hat{G}_{imp}(i\omega_n)\rangle_s x+\hat{\mathcal{G}}_0(i\omega_n)(1-x). \tag{A8}$$

We can now recompute the self-energy as

$$\hat{\Sigma}(i\omega_n)=\hat{\mathcal{G}}_0^{-1}(i\omega_n)-\hat{G}_{avg}^{-1}(i\omega_n). \tag{A9}$$

Figure 7 illustrates the complete DMFA algorithm. At the end of each iteration, we take the difference between the current self-energy matrix [the zeroth Matsubara frequency, $\hat{\Sigma}(i\omega_0)$, includes the largest contribution] and the one evaluated in the previous iteration. The loop ends whenever this difference is less than a desired tolerance.

APPENDIX B: FINDING T_c FROM THE MAGNETIZATION DATA

The partition function for a simple ferromagnetic mean-field model without any microscopic physics is

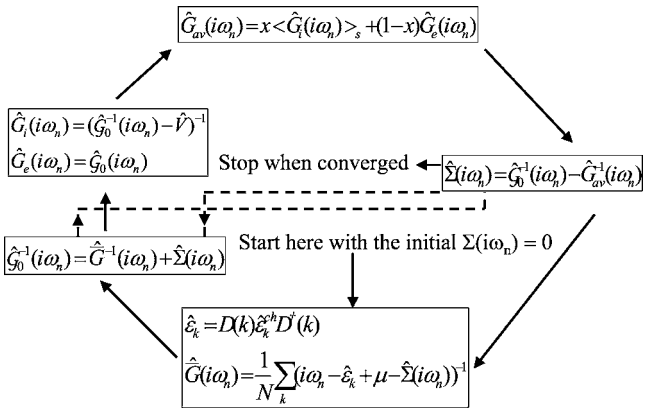

FIG. 7. The DMFA algorithm for the Green function.

$$\mathcal{Z}_{MF}=\int d\Omega_{\mathbf{S}}\exp(\beta\mathbf{S}\cdot\mathbf{H_{eff}}), \tag{B1}$$

where $|\mathbf{S}|=\frac{5}{2}$ for the local Mn ions and $\mathbf{H_{eff}}=\delta\mathbf{H^z}+\lambda\mathbf{M}$ with $\mathbf{M}=\langle\mathbf{S}\rangle$ the magnetization. The self-consistent equation for the magnetization,

$$M^z=\frac{1}{\mathcal{Z}_{MF}}\int d\Omega_{\mathbf{S}}S^z\exp[\beta\mathbf{S}\cdot(\delta\mathbf{H^z}+\lambda\mathbf{M})], \tag{B2}$$

becomes

$$M^z=\frac{1}{\beta H_{eff}}[\beta|\mathbf{S}|H_{eff}\coth(\beta H_{eff}|\mathbf{S}|)-1], \tag{B3}$$

where $H_{eff}=|\delta H^z|+\lambda M^z$ and $\lambda=3T_c/|\mathbf{S}|^2$. In the vicinity of the ferromagnetic phase transition temperature, T_c, the right side of Eq. (B3) simplifies to

$$M^z=\frac{|\mathbf{S}|^2}{3}\beta H_{eff}-\frac{|\mathbf{S}|^4}{45}(\beta H_{eff})^3. \tag{B4}$$

Therefore, close to the transition temperature, T_c, we are able to obtain an analytical expression for the magnetization as a function of temperature and magnetic field. We calculate T_c by fitting our DMFA data for M^z vs. T to these mean field formulas. The results for T_c were verified by its insensitivity to the field, with various fields given critical temperatures close to one another.

[1] R. N. Bhatt, M. Berciu, M. Kennett, and X. Wan, J. Supercond. **15**, 71 (2002); S. Sanvito, G. Theurich, and N. A. Hill, *ibid.* **15**, 85 (2002); B. Lee, T. Jungwirth, and A. H. MacDonald, Semicond. Sci. Technol. **17**, 393 (2002); T. Dietl *et al.*, *ibid.* **17**, 377 (2002); *Advances in Solid State Physics*, edited by B. Kramer (Springer, Berlin, 2003) (available at http://xxx.lanl.gov/abs/cond-mat/0306479).

[2] S. A. Wolf, D. D. Awschalom, R. A. Buhrman, J. M. Daughton, S. von Molnár, M. L. Roukes, A. Y. Chtchelkanova, and D. M. Treger, Science **294**, 1488 (2001).

[3] M. Linnarsson, E. Janzén, B. Monemar, M. Kleverman, and A. Thilderkvist, Phys. Rev. B **55**, 6938 (1997).

[4] J. Okabayashi, A. Kimura, O. Rader, T. Mizokawa, A. Fujimori, T. Hayashi, and M. Tanaka, Phys. Rev. B **58**, R4211 (1998).

[5] J. S. Blakemore, J. Appl. Phys. **53**, R123 (1982).

[6] G. Zaránd and B. Jankó, Phys. Rev. Lett. **89**, 047201 (2002).

[7] G. A. Fiete, G. Zaránd, and K. Damle, Phys. Rev. Lett. **91**, 097202 (2003).

[8] W. Metzner and D. Vollhardt, Phys. Rev. Lett. **62**, 324 (1989).

[9] E. Müller-Hartmann, Z. Phys. B: Condens. Matter **74**, 507 (1989).

[10] T. Pruschke, M. Jarrell, and J. K. Freericks, Adv. Phys. **42**, 187 (1995).

[11] A. Georges, G. Kotliar, W. Krauth, and M. Rozenberg, Rev. Mod. Phys. **68**, 13 (1996).

[12] A. Baldereschi and N. O. Lipari, Phys. Rev. B **8**, 2697 (1973).

[13] P. Kacman, Semicond. Sci. Technol. **16**, R25 (2001).

[14] D. W. Taylor, Phys. Rev. **156**, 1017 (1967); P. Soven, *ibid.* **156**, 809 (1967); P. L. Leath and B. Goodman, *ibid.* **148**, 968 (1966).

[15] N. Furukawa, J. Phys. Soc. Jpn. **63**, 3214 (1994); Proc. Conference on Physics of Manganites (1998) (available at http://xxx.lanl. gov/abs/cond-mat/9812066).

[16] H. Munekata, H. Ohno, S. von Molnár, A. Segmüller, L. L. Chang, and L. Esaki, Phys. Rev. Lett. **63**, 1849 (1989).

[17] H. Ohno, H. Munekata, T. Penney, S. von Molnár, and L. L. Chang, Phys. Rev. Lett. **68**, 2664 (1992).

[18] H. Ohno, A. Shen, F. Matsukura, A. Oiwa, A. Endo, S. Katsumoto, and Y. Iye, Appl. Phys. Lett. **69**, 363 (1996).

[19] A. Van Esch, L. Van Bockstal, J. De Boeck, G. Verbanck, A. S. van Steenbergen, P. J. Wellmann, B. Grietens, R. Bogaerts, F. Herlach, and G. Borghs, Phys. Rev. B **56**, 13103 (1997).

[20] H. Ohno, Science **281**, 951 (1998).

[21] D. Chiba, K. Takamura, F. Matsukura, and H. Ohno, Appl. Phys. Lett. **82**, 3020 (2003).

[22] K. W. Edmonds, P. Boguslawski, K. Y. Wang, R. P. Campion, S. N. Novikov, N. R. S. Farley, B. L. Gallagher, C. T. Foxon, M. Sawicki, T. Dietl, M. B. Nardelli, and J. Benholc, Phys. Rev. Lett. **92**, 037201 (2004).

[23] A. Chattopadhyay, S. Das Sarma, and A. J. Millis, Phys. Rev. Lett. **87**, 227202 (2001).

[24] E. J. Singley, R. Kawakami, D. D. Awschalom, and D. N. Basov, Phys. Rev. Lett. **89**, 097203 (2002).

[25] A. K. Bhattacharjee and C. Benoit à la Guillaume, Solid State Commun. **113**, 17 (2000).

[26] N. Furukawa, private communication.

[27] T. Dietl, H. Ohno, and F. Matsukura, Phys. Rev. B **63**, 195205 (2001).

[28] M. H. Hettler, M. Mukherjee, M. Jarrell, and H. R. Krishnamurthy, Phys. Rev. B **61**, 12739 (2000).